

Imaging seismic and aseismic plate coupling with interferometric radar (InSAR) in the Hikurangi subduction zone

L. Maubant¹, W. B. Frank¹, L.M Wallace^{2,3,4}, C. Williams⁵, Ian Hamling⁵

¹Department of Earth, Atmospheric and Planetary Sciences, Massachusetts Institute of Technology,
Cambridge, MA, USA

²University of Texas Institute for Geophysics, Austin Texas

³GEOMAR Helmholtz Centre for Ocean Research Kiel, Kiel, Germany

⁴Institute of Geosciences, Christian-Albrechts-Universität zu Kiel, Kiel, Germany

⁵GNS Science, Lower Hutt, New Zealand

Key Points:

- Integration of high-resolution displacement maps from radar imagery captures plate coupling at fine scales
- Estimates of plate coupling depend strongly on the time period over which surface velocities are measured
- Temporal variations in plate coupling highlight when and where slow slip dominates the slip budget

Corresponding author: Louise Maubant, maubant1@mit.edu

Abstract

The coupling at the interface between tectonic plates is a key geophysical parameter to capture the frictional locking across plate boundaries, and provides a means to estimate where tectonic strain is accumulating through time. Here, we use both interferometric radar (InSAR) and GNSS data to investigate the plate coupling of the Hikurangi subduction zone beneath the North Island of New Zealand, where multiple slow slip cycles are superimposed on the long-term loading. We estimate the plate coupling across the subduction zone over different observational periods (2, 4, and 10 years) targeting different stages of the slow slip cycles. Our results highlight the importance of the observational period when interpreting coupling maps, notably highlighting the temporal dependence of plate coupling. Through our analysis of multiple geodetic datasets, we demonstrate how InSAR provides powerful constraints on the spatial resolution of plate coupling, even in a region where a dense GNSS network exists.

Plain Language Summary

Plate coupling as a concept describes to what degree the boundaries between tectonic plates are frictionally locked and building up stress. Such accumulated stress (over many hundreds to thousands of years) will eventually be released in earthquakes, and therefore provides important information about the potential for future earthquakes. Our study uses satellite data to investigate how coupling between the plates along the Hikurangi subduction zone (New Zealand's largest and most dangerous plate boundary fault) changes with time. We analyzed Interferometric Synthetic Aperture Radar (InSAR) and Global Navigation Satellite System (GNSS) data to create maps showing the areas where the plates are stuck together (coupled) and where they move past each other (uncoupled). We show that the locations of plate coupling vary significantly for 2, 4 and 10-year timeframes, highlighting the importance of carefully considering the observation period when interpreting and comparing coupling maps.

1 Introduction

The coupling of tectonic plates describes to what degree the interfaces between them are frictionally locked and building up stress. This tectonic stress will eventually be released episodically once the strength of the fault is surpassed, with the style of slip depending on the

48 fault rheology. Driven by far-field plate motion with a constant velocity V_0 , the deformation
 49 rate along the plate interface between transient slip events is typically some fraction of the
 50 long-term plate motion rate (usually called the slip deficit rate, V). We quantify the degree
 51 of plate coupling γ (or the "coupling coefficient") as:

$$\gamma = \frac{V_0 - V}{V_0}. \quad (1)$$

52 The coupling coefficient varies between 0 and 1, where 1 implies a fully coupled plate in-
 53 terface and 0 suggests continuous motion at the long-term plate rate of one plate relative
 54 to the other. By utilizing surface velocity fields estimated from geodetic data, it is possible
 55 to recover the distribution of slip deficit rate (or backslip) and interplate coupling across a
 56 given fault geometry at depth (Savage, 1983).

57 The discovery of slow slip more than two decades ago (Dragert et al., 2001) has upended
 58 this simple conceptual model of a stationary (e.g., constant slip deficit rate) interseismic
 59 phase (e.g., Frank, 2016; Saux et al., 2022; Maubant et al., 2022; Mouchon et al., 2023).
 60 Geodetic observations across many tectonic plate boundaries have demonstrated how these
 61 transient slip events, which do not radiate seismic waves, can episodically release as much
 62 accumulated tectonic stress as major earthquakes ($>M7$) (e.g., Wallace, 2020; Graham et al.,
 63 2016; Maubant et al., 2020). Often (but not always) observed downdip of the seismogenic
 64 fault region, past work has highlighted how slow slip can interact with earthquakes by
 65 transferring stress onto seismogenically locked portions of the fault (Mazzotti & Adams,
 66 2004; Ito et al., 2013; Kato, 2004; Kaneko et al., 2018).

67 To assess coupling along subduction zones, surface velocities are typically estimated
 68 from campaign or continuous GNSS (Global Navigation Satellite System) surface motion
 69 at a given point in space. It follows that the density of the GNSS network then directly
 70 informs the potential spatial resolution of the recovered map of plate coupling. Modern SAR
 71 (Synthetic Aperture Radar) constellations directly tackle this issue of spatial resolution by
 72 measuring ground displacement over hundreds of kilometers with repeat times $<24d$ through
 73 Interferometric Synthetic Aperture Radar (InSAR) analysis. With each pixel of the radar
 74 images acting as its own geodetic sensor, this allows for dense spatial coverage of the surface
 75 velocity field that complements GNSS (Maubant et al., 2020). The precision of InSAR
 76 ground displacement is however much lower than that of GNSS, making it challenging to
 77 measure the displacement due to relatively small fault motions, such as a slow slip event.

Thanks to methodological improvements to InSAR processing, we can now constrain small velocities in the InSAR time series with amplitudes of mm/yr (Daout et al., 2019).

Here, we seek to quantify how plate coupling evolves in time and space across the Hikurangi subduction zone beneath New Zealand to capture the interplay between seismic and aseismic regions of frictional locking using both InSAR and GNSS observations. We focus on the Hikurangi margin, which accommodates the oblique subduction of the Pacific plate beneath Australian plate (Nicol et al., 2007), because it hosts multiple regions of slow slip across a range of depths (Wallace & Beavan, 2010; Wallace, 2020; Bartlow et al., 2014) and interact with both local and regional earthquakes (Wallace et al., 2017; Koulali et al., 2017). We consider the deep regions of slow slip to the south west that host major M7 slow slip events lasting 1-2 years, at depths of 25-50 km with a recurrence time of 4-5 years (Figure 1). We also take into account the northern Hikurangi margin’s East Coast slow slip events that rupture the shallow, offshore plate interface (Wallace et al., 2016), and are associated with tectonic tremor and increased earthquake activity (Wallace, Beavan, et al., 2012; Delahaye et al., 2009; Todd & Schwartz, 2016). We demonstrate how InSAR can provide high-resolution constraints on the spatial distribution of both aseismic and seismic locking considering different observational time periods during which surface velocities are estimated. With such an approach, we are able to capture the dynamic behavior of a subduction plate interface through time.

2 Geodetic data and analysis

We use the three components of daily positions of 155 continuous GNSS (Global Navigation Satellite System) stations, available between 2006 and 2022 and shown in Figure 1. The data are processed by GeoNet <https://www.geonet.org.nz> with GAMIT software (Herring et al., 2010). To focus on the interseismic geodetic signal, we corrected for co-seismic displacements caused by a March 2021 M7.3 intraslab event located 100 km off the northeast coast in the East Cape area (Figure 1) (Okuwaki et al., 2021). After correction of the co-seismic offset, we observe a post-seismic signal at a few stations that we did not correct (i.e, station WMAT in Figure 1), because the earthquake far from the coast generates a measureable signal at very few stations.

In addition to GNSS data, we use SAR imagery from the Sentinel-1 constellation operated by the European Space Agency. InSAR observations capture surface deformation

across large continuous swaths, providing the means to estimate the surface velocity at each of the pixels that make up every radar image; the images analyzed here have a swath width of about 250 km and a length of 400-500 km. Our analysis covers two tracks shown in Figure 1, A081 (ascending, with 183 images) and D175 (descending, with 154 images) that together cover a significant portion of the North Island of New Zealand from October 2014 to January 2022 with repeat times between 6-24 days; we show in Table S1 the number of images and interferograms analyzed in each track.

We use the NSBAS (New Small BASeline Subset) processing chain to process the interferograms that are then unwrapped and inverted to obtain a time series and capture the evolution of surface displacement (Thollard et al., 2021). To ensure robust estimates of the surface displacement time series and minimize potential biases linked to soil moisture and agricultural vegetation, we construct the interferogram network using a combination of short and long-temporal baselines (Mathey et al., 2022; Dodds et al., 2022). To enhance the signal-to-noise ratio, we filter the interferograms using a complex multi-looking with a window size of 64 pixels in range and 16 pixels in azimuth, resulting in a spatial resolution of approximately $160 \text{ m} \times 240 \text{ m}$. Tropospheric signals are corrected using the ERA-5 reanalysis weather model before unwrapping. Once unwrapped, the interferograms are inverted to obtain the surface displacement time series at each pixel (Doin et al., 2015; López-Quiroz et al., 2009).

3 Estimation of the surface velocity field during over three different time scales

Our objective is to quantify how the plate coupling, inferred from the surface velocity field estimated from the geodetic data, evolves during the interseismic period and superimposed slow slip event cycles. To achieve this, we investigate three different observational time periods (2006-2016, 2018-2022, and 2019.4-2021.3) spanning different portions of the slow slip cycles that occur at the Hikurangi subduction zone. The GNSS dataset covers more than 15 years (2006-2022), while our InSAR dataset covers only the 2014-2022 period. Wallace, Barnes, et al. (2012) utilized campaign GNSS velocities to estimate an average interseismic coupling between 1995-2008. Another study Wallace and Beavan (2010) investigated the coupling between slow slip events for the 2002-2010 period using the horizontal GNSS displacements corrected for observed slow slip. The geodetic data we use here covers a more recent time period with denser spatial coverage that also includes vertical motion,

sampling multiple (2-, 4-, and 10-year) time periods to investigate how plate coupling evolves in time.

The continuous GNSS time series from 2006-2022 capture multiple slow slip events at a range of spatiotemporal scales with minimal impact from seasonal environmental signals. Slow slip signals are also evident in our InSAR time series, including events from the Manawatu and Kapiti regions between 2014 and 2015. Because our InSAR time series does not record the beginning of the 2014-2015 deep slow slip event (Wallace, 2020), we are unable to accurately constrain this event with InSAR. We also avoid including the postseismic sequence of the 2016 Kaikōura earthquake and the margin-wide slow slip it triggered (Wallace et al., 2018; Jiang et al., 2018) within the time period of our velocity estimates. We thus use only the InSAR time series between 2018 and 2022 and April 2019 - March 2022. With these data considerations in mind, we estimate the surface velocities from GNSS and InSAR datasets over three different time periods:

- 10-year period between 2006 and 2016 constrained by GNSS displacements,
- 4-year period between 2018 and 2022 constrained by both GNSS and InSAR surface displacements, and
- 2-year period between April 2019 and March 2021 constrained by both GNSS and InSAR surface displacements.

The 2006-2016 period represents the time period before a major neighboring earthquake (the 2016 M7.8 Kaikōura earthquake), 2018-2022 represents the time between deep slow events that recur every four to five years, and April 2019 - March 2022 spans a time period between the major shallow slow events that occur every one to two years.

For each of the above time periods, we estimate a linear velocity V by fitting the following equation with a simple least-squares approach:

$$u(t) = Vt + u_0, \quad (2)$$

where u is the observed displacement, t is time, and u_0 is the static offset of the displacement time series. We estimate the three-component (North, East, and vertical) linear velocity V at each GNSS station. The velocities are projected into an upper plate reference frame using tectonic block Euler poles relative to the ITRF2014 (2014 International Terrestrial Reference Frame) from an elastic block model of the North Island and northern South Island Wallace,

Barnes, et al. (2012). Using velocities in a reference frame relative to the upper plate blocks allows us to invert for slip deficit on the plate interface without simultaneously inverting for tectonic rotation of the forearc which is a clear feature of the North Island GNSS velocity field (Wallace et al., 2004).

For each InSAR track, we generate a map of the surface velocity V at each pixel in the satellite’s line-of-sight (LOS) (Figure 3). The initial InSAR data is referenced to the ITRF14 reference frame (Stephenson et al., 2022), and we subsequently transform it to the upper plate reference frame used for the GNSS data (as described in the previous paragraph; Figure S2 and S3). To verify that our two datasets are in agreement, we compare the velocity obtained from GNSS data projected into the InSAR LOS direction to the InSAR-derived velocities. The datasets agree well with one another, exhibiting a correlation coefficient of 0.9 (Figure S5).

For the two shorter time periods, we observe higher vertical velocities during the 4-year and 2-year time periods compared to the 10-year period. This difference can be attributed to the larger slip deficit rates between slow slip events during the shorter time periods considered. Comparing the GNSS velocities over the 4-years and 2-year time periods, the only differences we observe are in the region of shallow slow slip events on the East Coast (Figure 2). This region hosts slow slip events that recur every 1-2 years, notably shorter than the 4-year time period. We do not however see a similar difference when comparing the InSAR-derived velocity maps at 2 and 4 years (Figure S6). This is likely because the amplitude of these events in the InSAR are small, InSAR data are more sensitive to the vertical component, and the signal can be hidden in the noise. Because of this observation, the insufficient number of acquisitions during the 2-year observation (maximum 50 dates), and the noise in our time series, we opted to use the 4-year InSAR velocities to constrain both our 2- and 4-years plate coupling models, while still using the 2- and 4-year GNSS velocities for the two respective models (Figure 2).

We estimate the associated error e of our linear velocities for both the GNSS and InSAR datasets as the root-mean-square between the model (Eq. 2) and the time series using the following:

$$e = \sqrt{\frac{\sum_{t=1}^N (u(t) - (Vt + u_0))^2}{N}} \quad (3)$$

where N is the number of observation epochs (eq. 2).

4 Geodetic inversion for the plate coupling

To retrieve the distribution of coupling on the Hikurangi subduction interface at depth, we utilize the linear velocities estimated during our three observational time periods to infer the slip rate along the subduction plate interface. We use the velocities estimated at all GNSS stations except those that are influenced by volcanic deformation within the Taupo Volcanic Zone of the central North Island, and volcanic-driven deformation at Whakaari/White Island. We now briefly describe our approach to invert for the slip velocity at depth; further details of our inversion are described in the Supplementary Information (Text S3).

We define the model *a priori* (m_0) as a plate interface coupled between 0 and 20 km depth (decreasing with the depth) and uncoupled further below. The poor data resolution near the trench with our terrestrial datasets cannot constrain the coupling near the trench. Consequently the chosen model *a priori* controls the recovered near-trench plate coupling (Figure S11, S12). We do not enforce positivity of the recovered slip velocity: a positive slip rate represents slip deficit (motion in the down-dip direction), while negative slip rates represent forward slip (slip in the updip direction as during a slow slip event). This allows us to obtain a model of the velocity field that accounts for elastic strain accumulation (or release) along the subduction interface for the three observational time periods considered (10, 4, and 2 years).

We invert for the slip rates along a 3D model geometry of the subduction interface (Williams et al., 2013) discretized into a triangle mesh (1746 patches). We use a linear least-squares algorithm with the regularization scheme of Radiguet et al. (2011) to perform the inversion, where two parameters, a damping coefficient (σ_{m0}) and a correlation length (λ), respectively control the stability and spatial smoothness of the recovered solution.

We then introduce a relative weight α to manage the influence of the two geodetic datasets, GNSS and InSAR, where α weights the relative contributions as captured by the covariance matrix of the data (Text S1). To evaluate the impact of each dataset, we separately inverted for the modeled plate coupling using either only GNSS or InSAR displacements (corresponding respectively to α values of 0.001 and 0.999 (Figure S8)). A comparison of the two inverted plate coupling maps shows that the spatial resolving power of InSAR is greater than that of the GNSS data, complementing the higher temporal resolution and lower uncertainties of the GNSS timeseries. We explore different α values to evaluate the best compromise, using a goodness-of-fit χ^2 metric (Figure S10). We choose $\alpha = 0.4$, as it

results in the lowest value of the cumulative misfit (sum of χ^2 values for InSAR and GNSS as described in Text S2). After determining the optimal weight, we explore different damping values (σ_{m0}) and correlation length values (λ) to assess the sensitivity of our model to the regularization (see Text S3). With the optimal α value determined, we find the compromise between the misfit of the model (χ^2) and its roughness, which was quantified using the L2 norm for these parameters (Figure S13).

Because the results of our inversion are expressed as slip deficits, we finally divide each patch with the associated value of V_{plate} (2-6 cm/yr; Figure S7) to estimate the coupling coefficient across the subduction zone. Undertaking a least-squares inversion of the surface displacement observations for slip on the plate interface, we obtain estimates of interplate coupling for each of three time periods that we investigate. The predicted surface velocities from the best-fitting slip models compare well with the observed surface velocity fields (Figure S9) for all three time periods.

5 Results and discussion

The recovered plate coupling map for each time period we investigate here are presented in Figure 4. Our 10-year coupling model most representative of the long-term interseismic phase is in good agreement with the model published by Wallace, Barnes, et al. (2012), which used campaign GNSS velocities estimated between 1995 and 2008. We observe low coupling values ($\gamma < 0.25$) depths > 25 km across the margin and an along-strike transition from high coupling coefficients beneath the southern North Island to a largely uncoupled interface beneath the northern and central margin. Such similar long-term coupling over more than two decades (1995-2022) suggests the interseismic phase is relatively stable over long time scales.

The observed surface velocities, which are generally towards the West corresponding to locking at depth, above the deep region of slow slip over the 2006-2016 period are slower relative to the upper plate than the 4- and 2-year velocities estimated at over periods shorter than the regional 4-5 year slow slip recurrence interval. This is not surprising as it is the signature of elastic strain accumulation observed between deep slow slip events in the Kapiti and Manawatu regions (Figure 1). This is captured in our 4- and 2-year coupling models, which aligns closely with past work Wallace and Beavan (2010) that examined coupling between slow slip events during the 2002-2010 period and highlights the stability of the

coupling between slow slip events through time. Compared to our 10-year coupling map, this region of coupling extends further downdip (Figure 4), corresponding well with the Kapiti and Manawatu slow slip events that happen at depth (Figure 4). This deep source region of slow slip however appears uncoupled with a null coupling coefficient once we consider our 10-year observational time period, suggesting that all of the accumulated slip deficit is fully relieved by deep slow slip during the 2006-2016 period; this period includes the 2008 Kapiti, the 2010-2011 Manawatu (Wallace & Beavan, 2010), the 2013 Kapiti, and the 2014-2016 Manawatu (Wallace et al., 2014) events.

We observe a difference in coupling within the deep slow slip region of Kapiti and Manawatu between the joint GNSS-InSAR models and those solely constrained by GNSS data at both 4 and 2 years. The joint model reveals a broad coupled region between 30 and 50 km depth, which corresponds to the Manawatu and Kapiti slow slip regions that were constrained previously by estimates of displacements during slow slip (Wallace, 2020) (Figure 4, S11). We note that our plate coupling model based only on GNSS data fails to capture this locked patch with the same level of spatial accuracy. This improved spatial resolution afforded by InSAR is particularly noticeable in areas where the GNSS network is sparse due to the exclusion of stations affected by volcanic signals. Our results thus demonstrate how InSAR can provide high-resolution constraints on plate coupling across a subduction zone, allowing for detailed identification of slow slip source regions (Figure S12). Despite the spatial resolving power of InSAR, the near-trench area of the Hikurangi subduction zone remains poorly resolved (Figure S11, S12). This suggests the importance of offshore geodetic instrumentation in accurately capturing the slip behavior within the tsunamigenic zone near the trench.

We remark that regions of slow slip are typically identified through inversion of static displacements during the slow slip event itself (Frank et al., 2015; Wallace, 2020). The estimation of surface velocities is however a more well constrained problem compare to measuring the displacement between two epochs, allowing us to take full advantage of the InSAR observations. While still possible for the largest slow slip events (Maubant et al., 2020), it would otherwise be challenging to identify where slow slip happens if we solely relied on measuring static displacements with InSAR data. Here we instead identify where slow slip occurs by constraining the slip deficit between slow slip events and comparing this with the longer-term interseismic coupling (Figure 4 and S14); this supposes that the slow slip source region is fully locked in between events. As an example, we map the cumulative

slip over one cycle in the deep slow slip region by differencing the predicted slip velocities of our 10-year and 4-year models, shown in Figure 4. We observe that the spatial distribution and maximum slip of about 18 cm corresponds well to past models of slow slip in this region (Williams & Wallace, 2015; Bartlow et al., 2014).

We also observe a difference in coupling over our three observational time periods in the East Coast region of shallow slow slip (Figure 4). During our shortest observational period, we see that the East Coast source region exhibits spatially variable plate coupling, with strong coupling only in the North and the South. Looking at the displacement captured at the coast in Figure 1 (e.g, MAKO), there are multiple slow slip events occurring at <1 yr time scales evident in the GNSS time series. These slow slip events are present within our three observational time periods and thus reduce the recovered coupling in all of our models, explaining this spatially variable coupling within the shallow slow slip source region. At longer time scales (10- and 4-year estimates of plate coupling), this region appears to be fully uncoupled, due to the fact that multiple, shallow east coast SSEs occurred during that period. Unsurprisingly, the East Coast region has a lower coupling ($\gamma < 0.30$) over 10 years compared to the 2-year and 4-year periods of observation, due to the relatively frequent (every 1-2 years) shallow SSEs.

We observe in Figure 4 an area of negative coupling near the trench in the East Coast region during the 4-year observation period. While the fact that we did not take into account the slow events in the area during this period would explain low or null coupling, it cannot explain negative coupling (more slip than slip deficit during the observational time period). Furthermore, we observe a relatively small coupled patch down dip of this negative coupling that is only present in the 4-year coupling map and not in the 2-year coupling map. We attribute this pair of coupled and uncoupled patches to deformation in the GNSS network due to an earthquake sequence in the neighboring Kermadec subduction zone in March 2021, where we were unable to correct the associated postseismic signal due to the relatively small geodetic signal of the earthquakes far from the geodetic network.

6 Conclusion

We demonstrate here how InSAR data together with GNSS positioning enables us to capture the spatiotemporal evolution of plate coupling in the Hikurangi subduction zone. We show how surface velocities estimated from InSAR time series significantly improves

the resolution of slip (deficit) at depth, especially in regions where GNSS coverage is sparse (Figure S8). We highlight that near-trench coupling remains poorly resolved, emphasizing the need for integration of offshore geodetic data (Figure S12). Our plate coupling models estimated over three different time periods (10, 4, and 2 years) are similar to past estimates of coupling constrained solely by GNSS (Wallace & Beavan, 2010; Wallace, Barnes, et al., 2012), but we highlight stark differences with increased spatial resolution of the deep slow slip source region and spatially varying coupling in the East Coast region that depends on the observational time period (Figure S14).

Our results suggest that the interseismic phase is not stationary due to the interplay of multiple slow slip cycles superimposed on the long-term, and likely seismic, coupling (Jolivet & Frank, 2020). This highlights that any estimate of plate coupling, derived from a given time period, is a snapshot of a continuously evolving plate interface (Frank, 2016; Mouchon et al., 2023). We note that the observed agreement between our 10-year model, which most likely represents the long-term interseismic phase, and a previously published interseismic coupling model suggests a relative stability of plate coupling over the past several decades. An advantage of considering several plate coupling models that span different slow slip cycles is that we are able to map out slow slip source regions with robust estimates of surface velocities, rather than noisier measurements of displacement offsets. This allows us to take full advantage of the InSAR dataset and its high spatial resolution, which otherwise lacks the signal-to-noise necessary to estimate the surface displacement offsets during slow slip events. Today, long-term coupling maps (≥ 20 years) can only be produced using GNSS data. With the increasing duration of current and future SAR constellations, it will be possible to integrate InSAR data into these estimates of long-term coupling to map slip at depth in high resolution. Even with current data limitations, we demonstrate how to resolve in high resolution the interplay of aseismic and seismic regions of coupling across the scale of a subduction zone.

7 Open Research

The GNSS data are in open access on <https://www.geonet.org.nz/data/types/geodetic>. Sentinel-1 data are available online <https://scihub.copernicus.eu>, we provide the results of the coupling maps, and InSAR and GNSS velocities (<https://zenodo.org/record/8124888>).

Acknowledgments

L.M., W.B.F, and L.W. acknowledge support from the National Aeronautics and Space Administration under Grant No. 80NSSC21K0874 issued through the Earth Sciences Division of the Science Mission Directorate. We thank Marie-Pierre Doin for discussions about the processing of the InSAR data.

References

- Bartlow, N. M., Wallace, L., Beavan, R. J., Bannister, S., & Segall, P. (2014). Time-dependent modeling of slow slip events and associated seismicity and tremor at the Hikurangi subduction zone, New Zealand. *Journal of Geophysical Research: Solid Earth*, 119(1), 734–753. doi: 10.1002/2013JB010609
- Daout, S., Sudhaus, H., Kausch, T., Steinberg, A., & Dini, B. (2019). Interseismic and Postseismic Shallow Creep of the North Qaidam Thrust Faults Detected with a Multitemporal InSAR Analysis. *Journal of Geophysical Research: Solid Earth*, 1–21. doi: 10.1029/2019JB017692
- Delahaye, E., Townend, J., Reyners, M., & Rogers, G. (2009). Microseismicity but no tremor accompanying slow slip in the hikurangi subduction zone, new zealand. *Earth and Planetary Science Letters*, 277(1-2), 21–28.
- Dodds, N., Daout, S., Walker, R., Begenjev, G., Bezmenov, Y., Mirzin, R., & Parsons, B. (2022). Interseismic deformation and strain-partitioning along the main köpetdag fault, turkmenistan, with sentinel-1 insar time-series. *Geophysical Journal International*, 230(3), 1612–1629.
- Doin, M.-P., Lasserre, C., & Grandin, R. (2015). InSAR Processing Sentinel 1 data Case study of subsidence in Mexico city. doi: 10.5270/Fringe2015.pp116
- Dragert, H., Wang, K., & James, T. S. (2001). A silent slip event on the deeper Cascadia subduction interface. *Science*, 292(5521), 1525–1528. doi: 10.1126/science.1060152
- Frank, W. B. (2016). Slow slip hidden in the noise: The intermittence of tectonic release. *Geophysical Research Letters*, 43(19), 10–125.
- Frank, W. B., Radiguet, M., Rousset, B., Shapiro, N. M., Husker, A. L., Kostoglodov, V., ... Campillo, M. (2015). Uncovering the geodetic signature of silent slip through repeating earthquakes. *Geophysical Research Letters*, 42(8), 2774–2779.

- Graham, S., DeMets, C., Cabral-Cano, E., Kostoglodov, V., Rousset, B., Walpersdorf, A.,
 ... Salazar-Tlaczani, L. (2016). Slow Slip History for the MEXICO Subduction
 Zone: 2005 Through 2011. *Pure and Applied Geophysics*, 173(10-11), 3445–3465. doi:
 10.1007/s00024-015-1211-x
- Herring, T., King, R., & McClusky, S. (2010). Introduction to gamit/globk. *Massachusetts
 Institute of Technology, Cambridge, Massachusetts*.
- Ito, Y., Hino, R., Kido, M., Fujimoto, H., Osada, Y., Inazu, D., ... Ashi, J. (2013). Episodic
 slow slip events in the Japan subduction zone before the 2011 Tohoku-Oki earthquake.
Tectonophysics, 600, 14–26. doi: 10.1016/j.tecto.2012.08.022
- Jiang, Z., Yuan, L., Huang, D., Zhang, L., Hassan, A., & Yang, Z. (2018). Spatial-temporal
 evolution of slow slip movements triggered by the 2016 Mw 7.8 Kaikoura earthquake,
 New Zealand. *Tectonophysics*, 744(June), 72–81. Retrieved from [https://doi.org/
 10.1016/j.tecto.2018.06.012](https://doi.org/10.1016/j.tecto.2018.06.012) doi: 10.1016/j.tecto.2018.06.012
- Jolivet, R., & Frank, W. (2020). The transient and intermittent nature of slow slip. *AGU
 Advances*, 1(1), e2019AV000126.
- Kaneko, Y., Wallace, L., Hamling, I. J., & Gerstenberger, M. C. (2018). Simple physical
 model for the probability of a subduction-zone earthquake following slow slip events
 and earthquakes: Application to the hikurangi megathrust, new zealand. *Geophysical
 Research Letters*, 45(9), 3932–3941.
- Kato, N. (2004). Interaction of slip on asperities: Numerical simulation of seismic cycles
 on a two-dimensional planar fault with nonuniform frictional property. *Journal of
 Geophysical Research: Solid Earth*, 109(12), 1–17. doi: 10.1029/2004JB003001
- Koulali, A., McClusky, S., Wallace, L., Allgeyer, S., Tregoning, P., D’Anastasio, E., &
 Benavente, R. (2017). Slow slip events and the 2016 Te Araroa Mw7.1 earthquake
 interaction: Northern Hikurangi subduction, New Zealand. *Geophysical Research Let-
 ters*, 44(16), 8336–8344. doi: 10.1002/2017GL074776
- López-Quiroz, P., Doin, M.-p., Tupin, F., Briole, P., & Nicolas, J. M. (2009). Time series
 analysis of Mexico City subsidence constrained by radar interferometry. *Journal of
 Applied Geophysics*, 69(1), 1–15. Retrieved from [http://dx.doi.org/10.1016/j
 .jappgeo.2009.02.006](http://dx.doi.org/10.1016/j.jappgeo.2009.02.006) doi: 10.1016/j.jappgeo.2009.02.006
- Mathey, M., Doin, M.-P., André, P., Walpersdorf, A., Baize, S., & Sue, C. (2022). Spatial
 heterogeneity of uplift pattern in the western european alps revealed by insar time-
 series analysis. *Geophysical Research Letters*, 49(1), e2021GL095744.

- 422 Maubant, L., Pathier, E., Daout, S., Radiguet, M., Doin, M.-P., Kazachkina, E., ...
 423 Walpersdorf, A. (2020). Independent component analysis and parametric approach for
 424 source separation in insar time series at regional scale: Application to the 2017–2018
 425 slow slip event in guerrero (mexico). *Journal of Geophysical Research: Solid Earth*,
 426 *125*(3), e2019JB018187.
- 427 Maubant, L., Radiguet, M., Pathier, E., Doin, M.-P., Cotte, N., Kazachkina, E., & Kos-
 428 toglodov, V. (2022). Interseismic coupling along the mexican subduction zone seen
 429 by insar and gnss. *Earth and Planetary Science Letters*, *586*, 117534.
- 430 Mazzotti, S., & Adams, J. (2004). Variability of near-term probability for the next great
 431 earthquake on the cascadia subduction zone. *Bulletin of the Seismological Society of*
 432 *America*, *94*(5), 1954–1959.
- 433 Mouchon, C., Frank, W. B., Radiguet, M., Poli, P., & Cotte, N. (2023). Subdaily slow
 434 fault slip dynamics captured by low-frequency earthquakes. *AGU Advances*, *4*(4),
 435 e2022AV000848.
- 436 Nicol, A., Mazengarb, C., Chanier, F., Rait, G., Uruski, C., & Wallace, L. (2007). Tectonic
 437 evolution of the active hikurangi subduction margin, new zealand, since the oligocene.
 438 *Tectonics*, *26*(4).
- 439 Okuwaki, R., Hicks, S. P., Craig, T. J., Fan, W., Goes, S., Wright, T. J., & Yagi, Y. (2021).
 440 Illuminating a contorted slab with a complex intraslab rupture evolution during the
 441 2021 mw 7.3 east cape, new zealand earthquake. *Geophysical Research Letters*, *48*(24),
 442 e2021GL095117.
- 443 Radiguet, M., Cotton, F., Vergnolle, M., Campillo, M., Valette, B., Kostoglodov, V., &
 444 Cotte, N. (2011). Spatial and temporal evolution of a long term slow slip event: The
 445 2006 Guerrero Slow Slip Event. *Geophysical Journal International*, *184*(2), 816–828.
 446 doi: 10.1111/j.1365-246X.2010.04866.x
- 447 Saux, J. P., Molitors Bergman, E. G., Evans, E. L., & Loveless, J. P. (2022). The role of slow
 448 slip events in the cascadia subduction zone earthquake cycle. *Journal of Geophysical*
 449 *Research: Solid Earth*, *127*(2), e2021JB022425.
- 450 Savage, J. C. (1983). A dislocation model of strain accumulation and release at a sub-
 451 duction zone. *Journal of Geophysical Research*, *88*(B6), 4984–4996. doi: 10.1029/
 452 JB088iB06p04984
- 453 Stephenson, O. L., Liu, Y.-K., Yunjun, Z., Simons, M., Rosen, P., & Xu, X. (2022). The
 454 impact of plate motions on long-wavelength insar-derived velocity fields. *Geophysical*

- 455 *Research Letters*, e2022GL099835.
- 456 Thollard, F., Clesse, D., Doin, M.-P., Donadieu, J., Durand, P., Grandin, R., ... others
 457 (2021). Flatsim: The form@ter large-scale multi-temporal sentinel-1 interferometry
 458 service. *Remote Sensing*, 13(18), 3734.
- 459 Todd, E. K., & Schwartz, S. Y. (2016). Tectonic tremor along the northern hikurangi
 460 margin, new zealand, between 2010 and 2015. *Journal of Geophysical Research: Solid*
 461 *Earth*, 121(12), 8706–8719.
- 462 Wallace, L. (2020). Slow slip events in new zealand. *Annual Review of Earth and Planetary*
 463 *Sciences*, 48, 175–203.
- 464 Wallace, L., Barnes, P., Beavan, J., Van Dissen, R., Litchfield, N., Mountjoy, J., ... Pondard,
 465 N. (2012). The kinematics of a transition from subduction to strike-slip: An example
 466 from the central new zealand plate boundary. *Journal of Geophysical Research: Solid*
 467 *Earth*, 117(B2).
- 468 Wallace, L., Bartlow, N., Hamling, I., & Fry, B. (2014). Quake clamps down on slow slip.
 469 *Geophysical Research Letters*, 41(24), 8840–8846.
- 470 Wallace, L., & Beavan, J. (2010). Diverse slow slip behavior at the hikurangi subduction
 471 margin, new zealand. *Journal of Geophysical Research: Solid Earth*, 115(B12).
- 472 Wallace, L., Beavan, J., Bannister, S., & Williams, C. (2012). Simultaneous long-term and
 473 short-term slow slip events at the hikurangi subduction margin, new zealand: Impli-
 474 cations for processes that control slow slip event occurrence, duration, and migration.
 475 *Journal of Geophysical Research: Solid Earth*, 117(B11).
- 476 Wallace, L., Beavan, J., McCaffrey, R., & Darby, D. (2004). Subduction zone coupling
 477 and tectonic block rotations in the north island, new zealand. *Journal of Geophysical*
 478 *Research: Solid Earth*, 109(B12).
- 479 Wallace, L., Hreinsdóttir, S., Ellis, S., Hamling, I., D’Anastasio, E., & Denys, P. (2018).
 480 Triggered Slow Slip and Afterslip on the Southern Hikurangi Subduction Zone Fol-
 481 lowing the Kaikōura Earthquake. *Geophysical Research Letters*, 45(10), 4710–4718.
 482 doi: 10.1002/2018GL077385
- 483 Wallace, L., Kaneko, Y., Hreinsdóttir, S., Hamling, I., Peng, Z., Bartlow, N., ... Fry, B.
 484 (2017). Large-scale dynamic triggering of shallow slow slip enhanced by overlying
 485 sedimentary wedge. *Nature Geoscience*, 10(10), 765–770.
- 486 Wallace, L., Webb, S. C., Ito, Y., Mochizuki, K., Hino, R., Henrys, S., ... Sheehan, A. F.
 487 (2016). Slow slip near the trench at the hikurangi subduction zone, new zealand.

- 488 *Science*, 352(6286), 701–704.
- 489 Williams, C. A., Eberhart-Phillips, D., Bannister, S., Barker, D. H., Henrys, S., Reyners,
490 M., & Sutherland, R. (2013). Revised interface geometry for the hikurangi subduction
491 zone, new zealand. *Seismological Research Letters*, 84(6), 1066–1073.
- 492 Williams, C. A., & Wallace, L. M. (2015). Effects of material property variations on
493 slip estimates for subduction interface slow-slip events. *Geophysical Research Letters*,
494 42(4), 1113–1121.

Figure 1: Tectonic setting of the Hikurangi subduction zone. The blue and red contours are 100mm contour slip intervals of slow slip events for 2002-2014 period (Wallace, 2020). The blue contours represent deep (25-40 km) and long-term (1-2 years) slow slip events that occurred in the Kapiti and Manawatu regions, while the red contours represent shallow (<15 km) and short-term (a few to several weeks) slow slip events that occurred offshore the East Coast. Black lines: crustal faults, Red dots: continuous GNSS stations (GeoNet network). Dashed dark black lines indicate the depths to the Hikurangi subduction interface in kilometers below sea level (Williams et al., 2013). The black boxes represent the footprint of the two tracks used in this study (Asc081 and Desc175). Beach balls is the moment tensor of the East Cape (Mw 7.3, 03/04/21). Below: Several GNSS time series from our study region (KAPT, TAKP, CKID, MAKO, and WMAT). The east displacement on TAKP and KAPT exhibits long-term transient events, including slow slip and afterslip following the Kaikōura earthquake in the Kapiti region. The east displacement on WMAT, MAKO, and CKID illustrates the interplay of multiple slow slip cycles. The red lines denote the Kaikōura (2016/11/14) and Kermadec (2021/03/04) earthquakes.

Figure 2: GNSS velocities over different time periods. a) Velocities between 2006 and 2016 (10 years). b) Velocities between 2018 and 2022 (between), corresponding to the period between deep a slow slip events. c) Velocities between April 2019 and March 2021, corresponding to the period between major slow slip events. The color scale indicates the magnitude of the velocities in millimeters per year for the vertical component. d) Difference between the 10-year (a) and 2-year (b) velocities.

Figure 3: Surface velocities over 2018-2022 between deep slow slip events. Top: a) and b) InSAR velocity maps for the respective ascending and descending tracks. The red dots on the ascending map represent the GNSS locations of TAKP and LEYL stations, which are shown below. Bottom: c) and d) East displacement time series respectively at TAKP and LEYL. The dashed red lines in c and d represent the estimated velocities over 2018-2022 (TAKP) and over the period April 2019 - March 2021 (LEYL). e) and f) Comparison of the A081 track displacements (blue dots) and the GNSS projected into Line-Of-Sight (LOS) (black dots). g) and h) Comparison of the D175 track displacements (blue dots) and the GNSS projected into LOS (black dots). The blue lines in these four panels represent a smoothing of the InSAR displacements over three epochs.

Figure 4: Plate coupling maps of the Hikurangi subduction zone for the three analyzed time periods. a) Coupling between deep slow slip events estimated over 4 years using InSAR and GNSS. b) Coupling between major deep and shallow slow slip events estimated over 2 years using InSAR and GNSS. c) Coupling representative of the interseismic period over 10 years using only GNSS data. The blue lines are the slip contour of the SSEs between 2002 and 2014, black lines are the footprint of the two InSAR tracks. d) Profiles of the coupling coefficient as a function of depth along the AA' and BB' profiles shown in c. The orange, blue and red lines are respectively the coupling over the 10-, 4-, 2-year periods. Red squares are the slow slip events regions e) Difference in coupling over 4 years between the InSAR-only and the GNSS-only models. f) Difference of slip deficit over 4 years, corresponding to one deep slow slip cycle, using the velocities predicted by our 10- and 4-year models. Unresolved patches are transparent using the resolution matrix of the 10-yr model.

Figure 1.

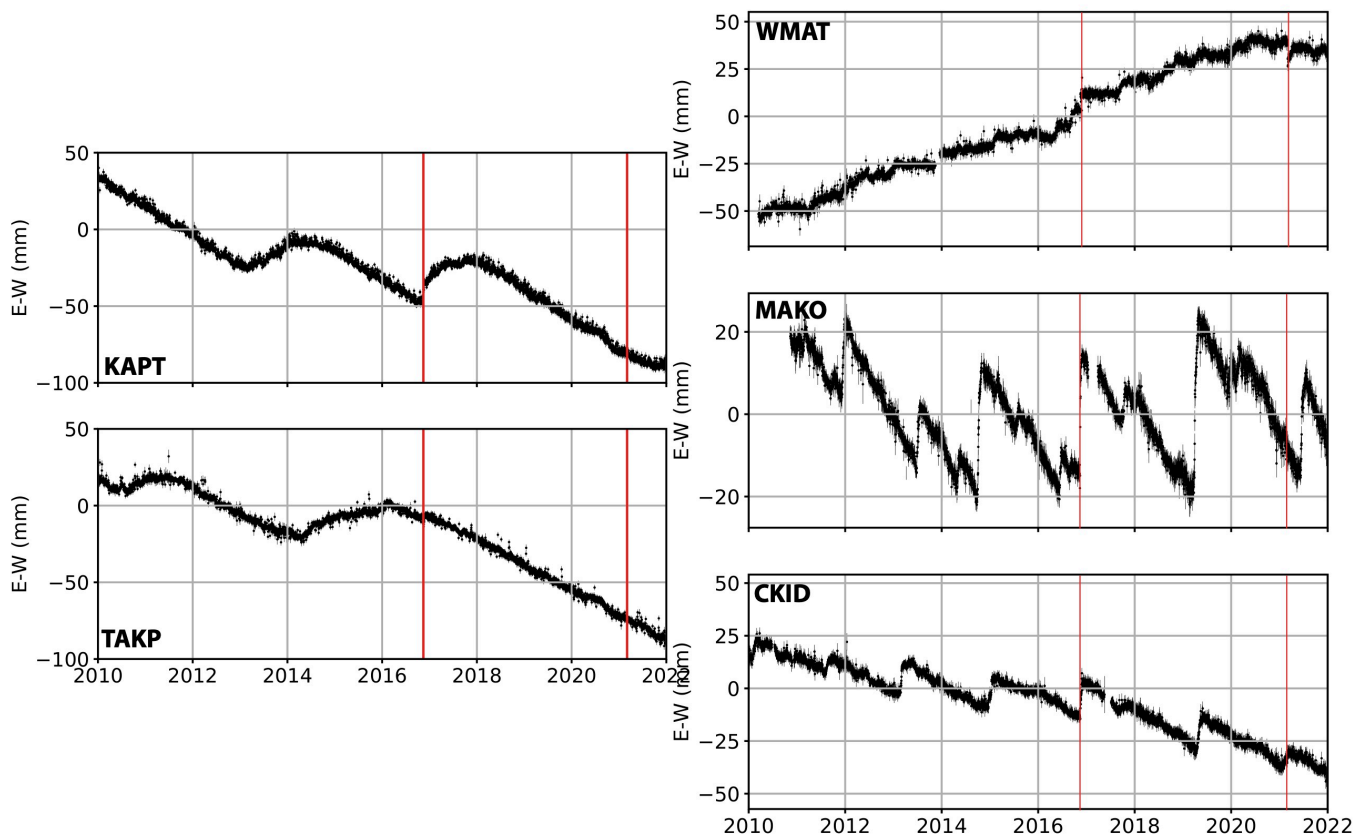
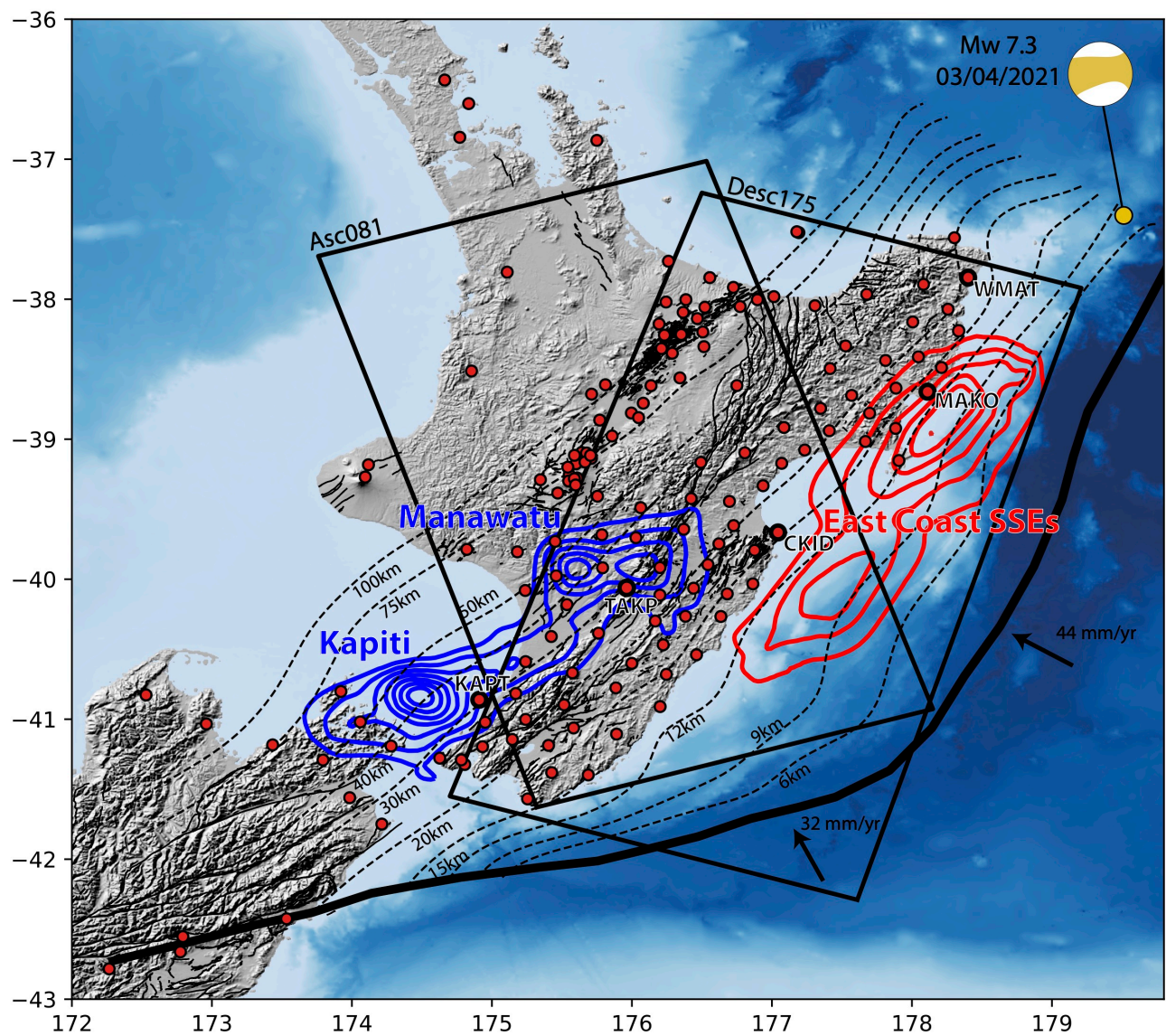


Figure 2.

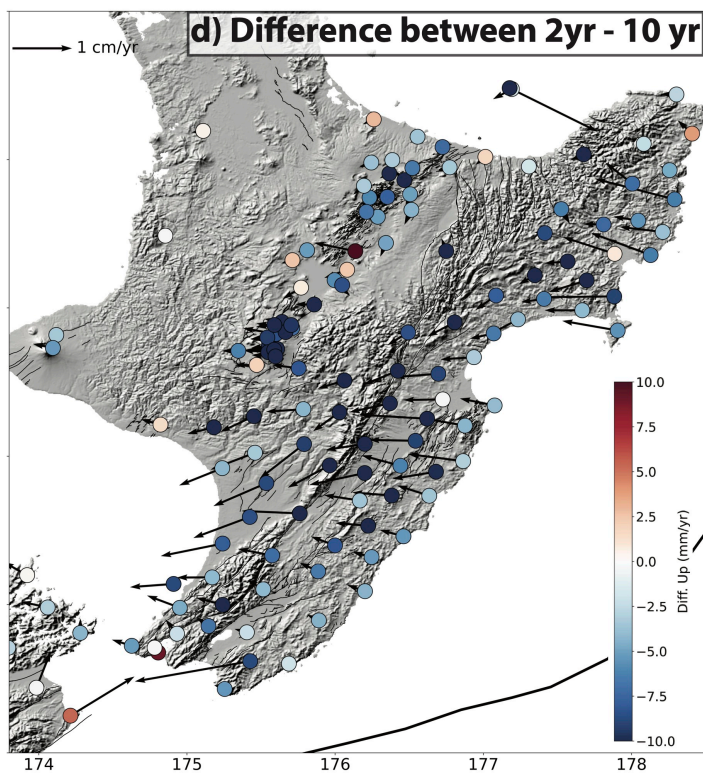
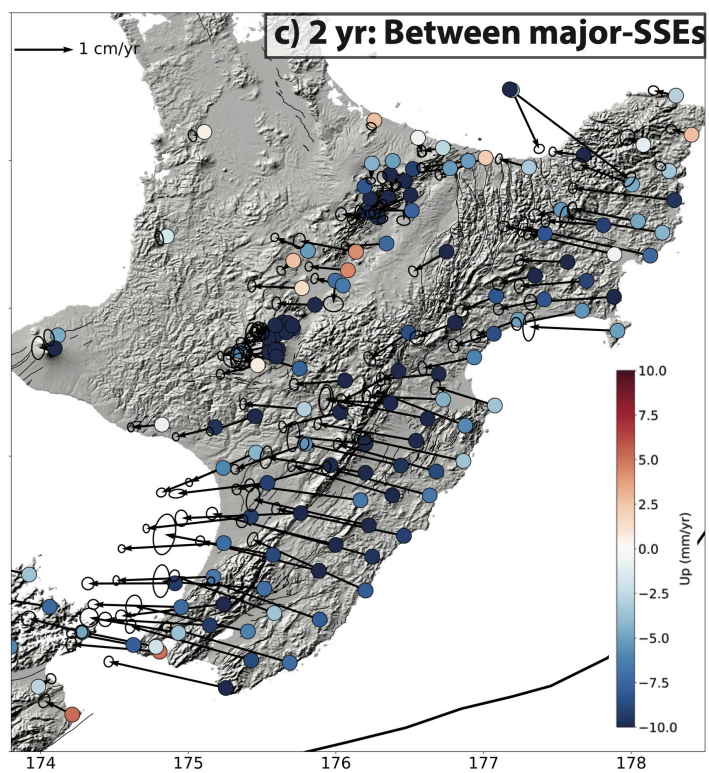
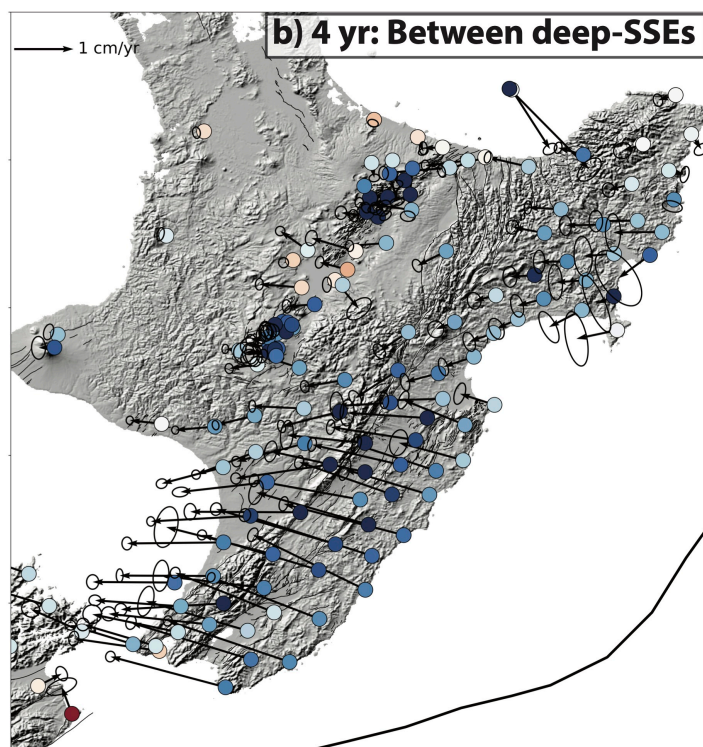
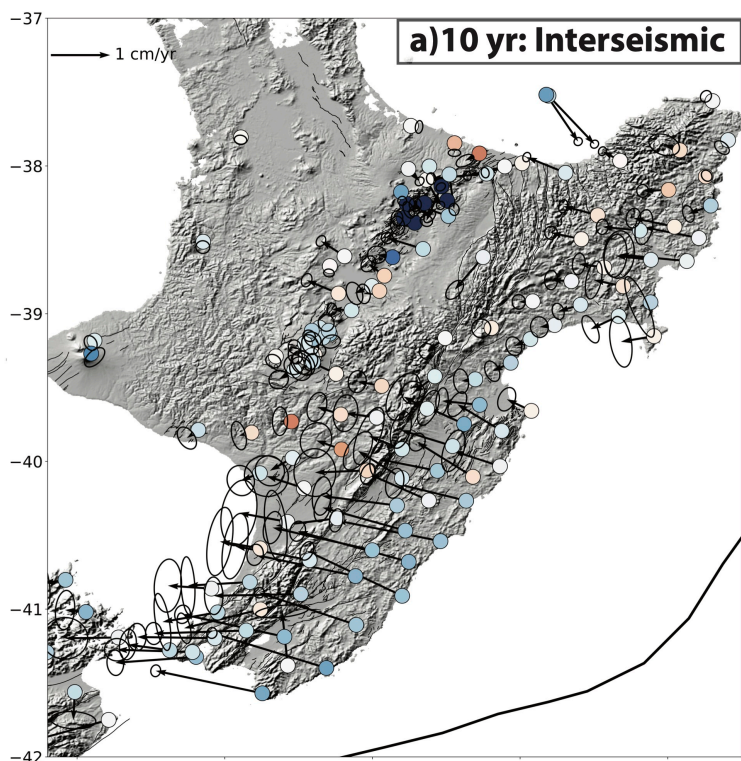


Figure 3.

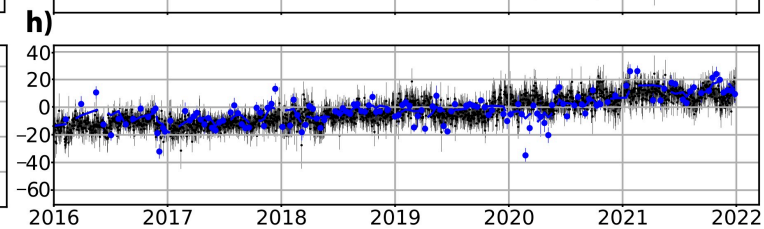
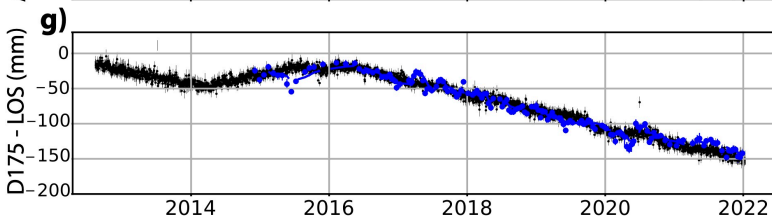
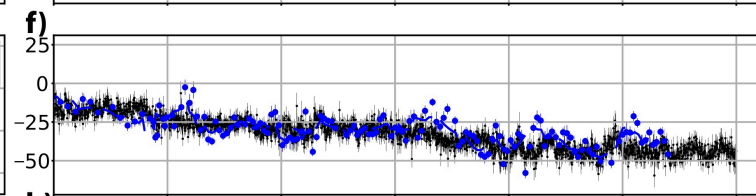
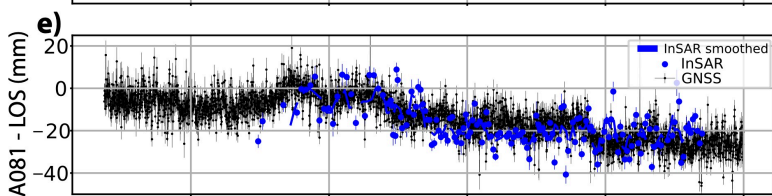
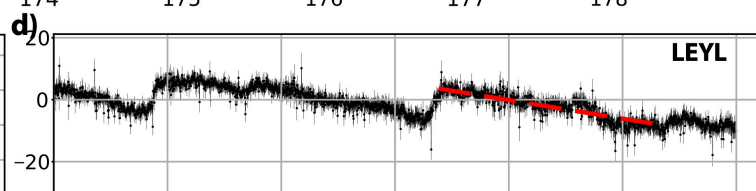
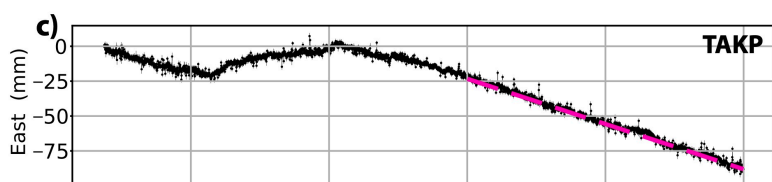
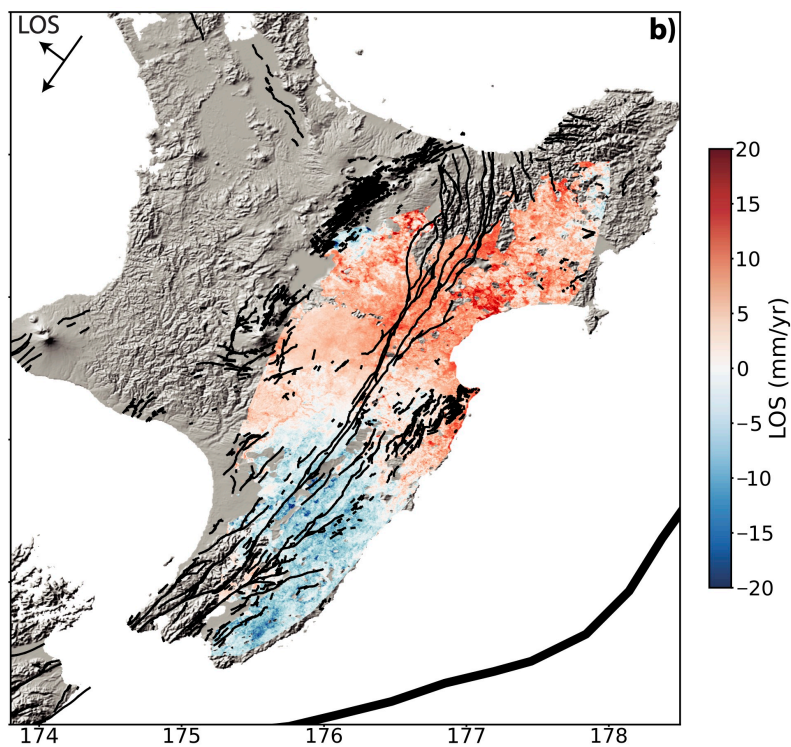
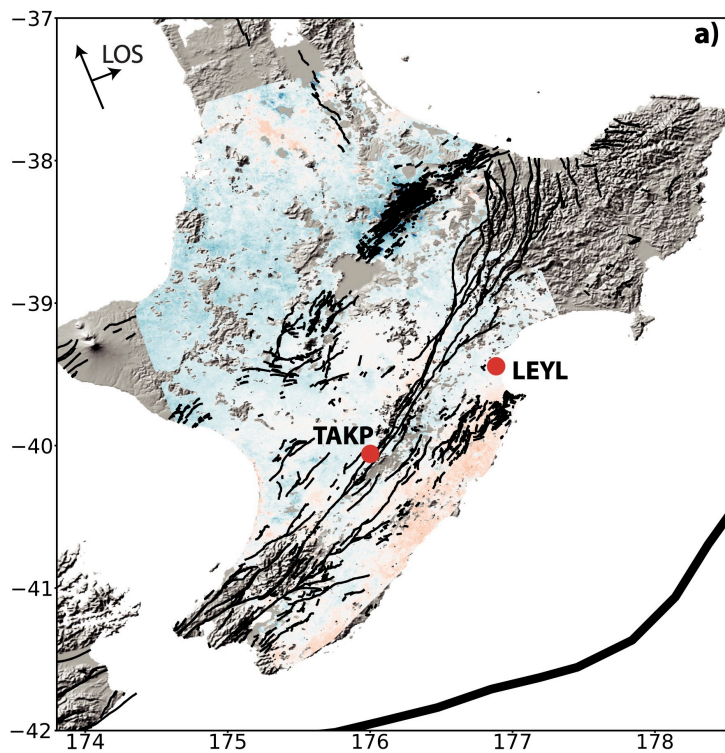


Figure 4.

